

# Estimation of Optimal Blank Holder Force Trajectories in Segmented Binders Using an ARMA Model

**Neil Krishnan**

Research Assistant  
e-mail: n-krishnan@northwestern.edu

**Jian Cao\***

Associate Professor  
Mem. ASME  
e-mail: jcao@northwestern.edu

Department of Mechanical Engineering,  
Northwestern University,  
Evanston, IL-60208

*Sheet metal forming is one of the most important and frequently used manufacturing processes in industry today. One of the key parameters affecting the forming process is the blank holder force (BHF). In the past, researchers have demonstrated the advantages of varying the blank holder force during the forming process, that is, the two primary modes of failure in sheet metal forming (wrinkling and tearing) are avoided. This gives rise to improved formability, higher accuracy and better part consistency. In recent years, researchers have also shown increasing interest in forming processes where the blank holder force is varied spatially with the help of segmented binders or flexible binders. In this paper, we have combined the above two aspects and used a robust method to determine the blank holder force trajectories for a non-circular part using segmented binders. The proposed strategy is verified by implementing it into a finite element simulation. Binder force is treated as a system input. The displacement of the binder is used as a measure of the tendency to wrinkle, and is therefore treated as a system output. The parameters of the system are continuously identified and updated using a deterministic Auto-Regressive Moving-Average model (ARMA). The model is then used to control the binder displacement to a prescribed value by adjusting the system input, i.e., the binder force. In this manner, individual binder force profiles for each of the segmented binders are obtained. Due to the generic nature of the ARMA model, the strategy proposed in this paper can be applied to a variety of forming problems, making it a robust approach. [DOI: 10.1115/1.1616948]*

## 1 Introduction

In a deep drawing process, the blank is deformed into its final desired shape by displacing a punch into a die and deforming the central region of the blank. The punch force deforms the blank by straining it against a constraint which is created by clamping the blank between a die and a blank holder along its periphery. The force used to clamp the blank between the die and blank holder is called the blank holder force (BHF). The blank holder force can be varied to achieve many desired objectives, from preventing the occurrence of tearing or wrinkling, and therefore, increasing the draw depth [1–3], to controlling springback [4,5]. The blank holder force can also be varied spatially, by employing segmented binders, flexible binders and local adaptive controllers [6–10].

Variation of blank holder force (BHF) can be determined *a-priori*, as applied in an open-loop manner, or by using a feedback loop, as a result of feedback control. One of the first examples of work done on blank holder force control was that of Hardt and Lee [11]. Using the general concept of a safe region between wrinkling and tearing, they proposed two closed-loop control strategies for a conical cup forming. The first method was designed to maintain a constant blank holder displacement, allowing a limited amount of flange wrinkling. The blank holder force was kept at the minimum necessary to prevent buckling in the unsupported region and also to prevent tearing. The second approach tried to control the binder force by regulating the volume of material entering the die cavity, through a generalized thickness parameter ( $t^*$ ). The conclusion drawn was that the strategies did

not appreciably increase the maximum cup height, but did significantly reduce the sensitivity of this maximum value to changes in the blank holder control variable.

Kergen and Jodogne [12,13] performed studies aimed at determining minimum BHF curve trajectories for various steels, based on a wrinkle detection system that measured the distance between the die and the blank holder in a cylindrical cup forming. The authors found that the measured BHF trajectories and the minimum BHF obtained from experiments varied significantly with variations in the types and properties of steels being tested. Hirose et al. [14] showed the success of an increasing linear combination BHF pattern in preventing the formation of wrinkles in an automobile panel. The authors further concluded that if a decreasing, linear combination BHF trajectory is used, body wrinkles are not suppressed.

Other researchers have reported favorable results obtained with decreasing BHF profiles. Kiri et al. [15], who also tested different linear combination patterns of BHF in panel formation, concluded that a decreasing BHF scheme was the optimum approach. Ahmetoglu et al. [16] obtained a different set of results. The authors employed computer simulation in the drawing of a round cup, in which three variables (punch force, radial stress and thickness strain) were used to control the blank holder force during simulation. The authors smoothed the results into a single decreasing BHF trajectory, which was then used to draw a cylindrical steel cup. This decreasing trajectory was used to successfully increase the draw depth over the case of a constant binder force. Ahmetoglu et al. [17] further examined decreasing binder force trajectories with regard to the deep drawing of rectangular parts from aluminum alloy 2008-T4. Their experiments indicated that a decreasing binder force significantly reduced the amplitude of wrinkles, while avoiding the fracture associated with high BHF values.

\*Corresponding author.

Contributed by the Manufacturing Engineering Division for publication in the JOURNAL OF MANUFACTURING SCIENCE AND ENGINEERING. Manuscript received Aug. 2002; Revised March 2003. Associate Editor: R. Smelser.

Another noteworthy example of blank holder force control is the work of Sim and Boyce [18]. The authors performed axisymmetric cup forming process simulations based on the tangential force and normalized average thickness trajectories. These models yielded numerical results for BHF trajectories that were later employed to increase the height to which cups could be drawn. Cao and Boyce [3] built upon this work to develop a novel approach to determine a variable BHF trajectory. The authors performed finite element simulations with PI control of the blank holder force. They were able to calculate a BHF trajectory having a combined upward and downward portion that showed a 16% increase in forming height over the results obtained by the best constant binder force case.

Recently, experiments by Siegert and Ziegler [19] have shown that the onset of wrinkling in a blank drawn with a pulsating BHF occurs at a displacement similar to that obtained under a constant BHF equal to the maximum force of pulsation. The reduction in the friction force achieved due to the pulse allows more material flow to take place, thus reducing the chances of tearing.

Hsu et al. [20] proposed an approach for modeling sheet metal forming for process controller design. They developed a process model for U-channel forming, i.e., a mathematical relationship between the blank holder force and the punch force was determined and validated experimentally. Characterization of model uncertainty due to blank size, sheet thickness, material properties and tooling shape was also studied. The process model was shown to be effective in describing the forming process.

Blank holder force variation has also been used to effectively control springback in sheet metal forming. Using the concept of intermediate restraining, Cao et al. [4] used a neural network to determine a stepped binder force trajectory that was used to minimize springback and also obtain consistent results in channel forming, despite the presence of material variations and different lubricants. The approach was shown to be robust and applicable to a wide range of materials and process conditions. Liu et al. [5] used a similar approach in the forming of U-shaped parts and concluded that forming quality was improved when a variable binder force trajectory was used.

The use of segmented tooling and flexible binders is an area of sheet metal forming that has also been gaining prominence in recent years. The advantages of spatial variation of blank holder force have been cited in several research endeavors. One of the first examples of segmented binder tooling can be found in Siegert et al. [6]. The authors discussed a deep drawing apparatus developed at the Institute of Metal Forming Technology in which the lower binder is composed of eight individual segments, four corner segments and four straight segments. Each of these segments is powered by its own separate hydraulic cylinder. This allows an optimal blank holder force to be applied to individual regions of the blank. Thus, the blank holder force can be varied spatially in such a manner that individual segments of the binder can apply optimal values of blank holder force as desired.

Neugebauer et al. [7] performed studies using flexible binders and multiple draw pins. Their experimental set up consisted of an asymmetric part and a binder which had 12 draw pins distributed evenly along its periphery. The draw pins could be used to apply different values of binder force. They studied four cases, a rigid binder (80 mm thick) with a uniform pin force, a rigid binder with a non-uniform pin force, a flexible binder (30 mm thick) with a uniform pin force and a flexible binder with a nonuniform pin force. Although no major difference was observed in the two cases where a rigid binder was used, the case of a flexible binder with constant pin force increased the maximum achievable drawing depth from 70 mm to 90 mm. In the case of a flexible binder with non-uniform pin force, draw depths up to 110 mm were achieved.

Doege et al. [8] proposed an innovative concept in which the blank holder is designed as an elastically deformable thin steel plate. The authors used FEM analysis to determine the plate thickness and the location of support elements holding the binder. They

performed experiments at various binder force values to estimate a “safe working area.” The authors were able to show that the safe working area for a part is larger with a pliable blank holder and it moves towards higher blank holder force values. Furthermore, it was shown that the distribution of pressure on the blank was more uniform, thus giving rise to improved part quality.

Kinsey et al. [9] proposed a novel method of forming tailor welded blanks that incorporated a segmented die with local adaptive controllers. The local adaptive controllers consisted of hydraulic cylinders positioned in such a manner as to create an additional constraint within the forming area. The position of this constraint is selected so as to minimize the weld line movement and therefore reduce the strain developed in the thinner material. Experiments performed on an asymmetric part showed that this method of forming helped increase the draw depth by 20% over the conventional case.

All these studies indicate that spatial and temporal variations of BHF can provide improved results in sheet metal forming. However, there exists no consensus on the procedure to be followed in order to obtain optimum BHF trajectories. The objective of this paper is to design a strategy that can be applied universally to all part geometries and material models where wrinkling failure is of concern. For this purpose, the use of an ARMA model is investigated. The basic format of the ARMA model can be found in Graupe et al. [21] and Kay et al. [22] and will be reviewed in section 2. The ARMA model is used in various forms of time series analysis and system identification problems. Fassois et al. [23] used the ARMA model in the design of a fast algorithm for on-line machining process modeling and adaptive control.

Due to the generic nature of the ARMA model, it is an ideal candidate for use in problems with segmented or flexible binders. Also, since the model does not require any *a-priori* knowledge of the system, it can be easily applied to a variety of part geometries, tooling conditions and material models. The main technical challenges of this research work are to lay out a general strategy for determining the optimal binder force in sheet metal forming where flange wrinkling is the major concern, to show that the ARMA model can be effectively used to achieve this task and to demonstrate that the ARMA model is a robust approach which can be used for different applications. In subsequent sections of the paper, the basics of the ARMA model will be presented, including a section on the determination of the model order and delay. The ARMA model is then implemented in FEM simulations and the ensuing results are discussed. The paper ends with a brief section outlining our conclusions.

## 2 The ARMA Model

The control of blank holder force in a sheet metal forming operation can be achieved in several ways. Here, in this paper, the strategy adopted is to use the ARMA model and vary the blank holder force in multiple blank holder force scenarios so as to maintain a constant, pre-determined wrinkling amplitude under the blank holder. The displacement of the blank holder is an index that measures the flange wrinkling amplitude of the blank, and therefore, it is treated as the system output. The blank holder force can be varied to suppress this wrinkling tendency and is treated as the corresponding system input.

The ARMA model can be represented, in its simplest form, as:

$$\begin{aligned} \mathbf{y}_n &= \mathbf{a}_1 \mathbf{y}_{n-1} + \mathbf{a}_2 \mathbf{y}_{n-2} + \dots + \mathbf{b}_0 \mathbf{x}_{n-d} + \mathbf{b}_1 \mathbf{x}_{n-d-1} + \dots \quad (1) \\ &= \sum_{p=1}^s \mathbf{a}_p \mathbf{y}_{n-p} + \sum_{q=0}^t \mathbf{b}_q \mathbf{x}_{n-q-d} \quad (2) \end{aligned}$$

where  $\mathbf{x}$  represents system input vector, and  $\mathbf{y}$  is the system output vector. The subscripts  $n, n-1, \dots$  represent the sampling instances,  $s$  and  $t+1$  are the number of autoregressive and moving-average terms respectively. The letter  $d$  represents the delay in sampling intervals between inputs and outputs, and  $\mathbf{a}_p, \mathbf{b}_q$ , are the system parameter matrices.

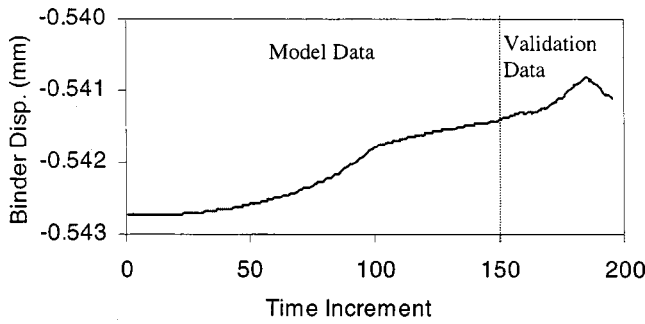


Fig. 1 Binder displacement data used to determine model order and delay

### 3 Determination of Model Order and Delay

The first step in using the ARMA model for BHF variation is to determine the appropriate order and delay of the model. The order refers to the number of autoregressive terms and the number of moving average terms used in the model ( $s$  and  $t$  in Eq. (2)). The delay is the time delay between inputs and outputs ( $d$  in Eq. (2)). If the number of terms used in the model is less than optimal, the model will fail to capture the system response accurately. On the other hand, if the number of terms used is more than required, the model may be successful in reproducing the system behavior, but additional system parameters need to be estimated. For this purpose, the System Identification Toolbox in MATLAB was used. A finite element simulation was conducted to obtain values of binder force and binder displacement. The data was divided into two sets, *model data* which was used to estimate the parameters of the system and *validation data* which was used to evaluate the performance of the model. Figures 1 and 2 show the data plots from one of the binders (Binder 2 in Fig. 7(a)). The data up to the time increment 150 is used as model data and the data from the time increment 151 until the end is used as validation data. The BHF trajectory selected here is arbitrary, the only requirement being that it varies sufficiently to produce a response that can be used effectively in system identification. Using the model data, various models are selected and the system parameters are determined. These parameters are then used to predict results and these results are compared to the validation data. The solid line in Fig. 3 shows the results for the optimal case where we have two autoregressive terms ( $s=2$ ), two moving average terms ( $t=2$ ) and no time delay ( $d=0$ ), i.e.,

$$BD_n = \theta_1(BD_{n-1}) + \theta_2(BD_{n-2}) + \theta_3(DBF_n) + \theta_4(DBF_{n-1}) \quad (3)$$

where

$n$ =increment number,

$BD_i$ =binder displacement in the  $i$ th increment,

$DBF_i$ =binder force change in the  $i$ th increment,

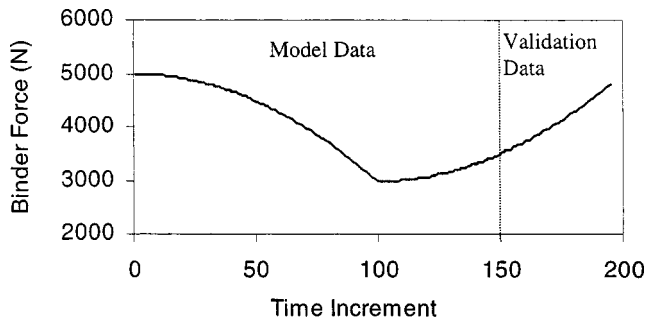


Fig. 2 Binder force data used to determine model order and delay

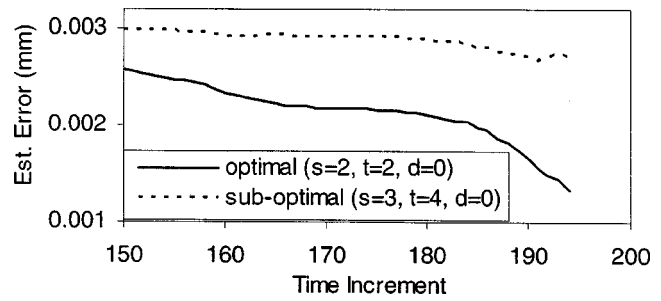


Fig. 3 Estimation error of validation data for optimal and sub-optimal model structures

$\theta_i$ =parameters of the system, ( $i=1,2,3 \dots$ )

The results are shown in terms of estimation error,  $err$ , which is defined as:

$$err = y - \hat{y} \quad (4)$$

where  $y$  is the actual output and  $\hat{y}$  is the predicted output. As a comparison to Fig. 3 we provide the estimation error plots for models with sub-optimal orders and delays. The values of  $s$ ,  $t$ , and  $d$  specified in Figs. 3 and 4 refer to Eq. (2). Figure 4 clearly shows the scenario where the model is unable to capture the system response accurately. The model structure is:

$$BD_n = \theta_1(BD_{n-1}) + \theta_2(DBF_{n-1}) \quad (5)$$

The estimation error values are high, almost of the order of the binder displacement itself. Figure 3 also shows the result for a model of a higher order represented by the dotted line. The model structure is:

$$BD_n = \theta_1(BD_{n-1}) + \theta_2(BD_{n-2}) + \theta_3(BD_{n-3}) + \theta_4(DBF_n) + \theta_5(DBF_{n-1}) + \theta_6(DBF_{n-2}) + \theta_7(DBF_{n-3}) \quad (6)$$

Increasing the order beyond the optimal value does not give any noticeable increase in the accuracy of the result. The effort of estimating the additional parameters merely introduces an increase in computational time. The results demonstrated here are for a model with one variable. However, the same analysis can be extended to a case which entails multiple variables.

### 4 Comparison of PI Control V/S ARMA Model

The blank holder force can be varied in an open loop or a closed loop manner and there are several strategies that can be applied to achieve this control mechanism. For example, proportional-integral (PI) control has been used in past research to vary the blank holder force [3]. However, there are certain disadvantages in using PI control, which can be overcome by using the ARMA model. In this section, we present a comparison of the two strategies.

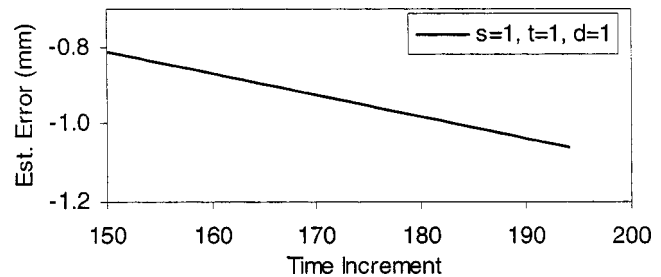


Fig. 4 Estimation error of validation data for a sub-optimal model structure

**Binder force estimation using PI control:** The PI controller as applied to binder force control is illustrated by the expression in Eq. (7). The desired binder force is adjusted as follows for each increment in the simulation,

$$BF_{n+1} = BF_n + K_p(e_n - e_{n-1}) + K_i(e_n) \quad (7)$$

where

$BF_{n+1}$  = desired binder force for the next increment

$BF_n$  = actual binder force in the current increment

$K_p$  = proportional gain

$K_i$  = integral gain

$e_n$  = error between target binder displacement and binder displacement in the current step

$n$  = increment number

This method of control has several advantages. It is simple and easy to implement and it does not involve a lot of computation. It has also been used in the previous work to control binder force in forming simulations of a circular cup [3]. The disadvantages of this control method is that the values of proportional gain and integral gain have to be determined by the user. The performance of the system depends on these values. The controller is not robust in the sense that the gains have to be adjusted for each particular system. It is precisely to overcome these difficulties that a strategy based on an ARMA model is recommended.

**Binder Force Variation using an ARMA model:** In this method, the relationship between the binder displacement and the binder force is expressed in the form of an autoregressive, moving-average model. Therefore, for each increment,

$$BD_n = \theta_1(BD_{n-1}) + \theta_2(BD_{n-2}) + \theta_3(DBF_n) + \theta_4(DBF_{n-1}) + \theta_5(T_n) \quad (8)$$

where

$n$  = increment number,

$BD_i$  = binder displacement in the  $i$ th increment,

$DBF_i$  = binder force change in the  $i$ th increment,

$\theta_i$  = parameters of the system, ( $i = 1$  to 5),

$T_n$  = normalized punch displacement,

The term " $T_n$ " is added to the expression to capture the dependence of the binder displacement on punch displacement, particularly at low values of blank holder force. Since the values of binder displacement and blank holder force are outputs and inputs in the ARMA model, the parameters of the system can now be evaluated using a recursive least-squares algorithm. Once the parameters are obtained, the model is completely defined, and this model can then be used to estimate the blank holder force required to maintain a constant target binder displacement. The recursive least-squares algorithm is implemented as follows:

$\theta_n$  = parameters of the system at time increment  $n$

$\theta_n = [\theta_1 \theta_2 \dots \theta_5]^T$

$\psi_n = [BD_{n-1} \ BD_{n-2} \ DBF_n \ DBF_{n-1} \ T_n]$

$P_n$  = system information matrix ( $5 \times 5$ )

$$\theta_n = \theta_{n-1} + \frac{P_{n-1} * \psi_n}{\lambda + \psi_n^T * P_{n-1} * \psi_n} [BD_n - \psi_n^T * \theta_{n-1}] \quad (9)$$

$$P_n = \frac{1}{\lambda} P_{n-1} - \frac{P_{n-1} * \psi_n * \psi_n^T * P_{n-1}}{\lambda + \psi_n^T * P_{n-1} * \psi_n} \quad (10)$$

Here,  $\lambda$  is the forgetting factor and it is selected to be slightly smaller than one. The algorithm is initialized by selecting  $\theta_0 = 0$ ,  $P_0 = \alpha I$  ( $\alpha \gg 0$ ). In this paper, we set  $\lambda = 0.99$  and  $\alpha = 10$ . The values of  $\lambda$  and  $\alpha$  are selected based on recommended acceptable values for convergence in the literature [24].

For the purpose of comparison, a simple MATLAB program was used to generate an objective function and a control system. The objective function is a relationship used to simulate the binder displacement based on different inputs of binder force and normalized punch displacement. The objective function was chosen

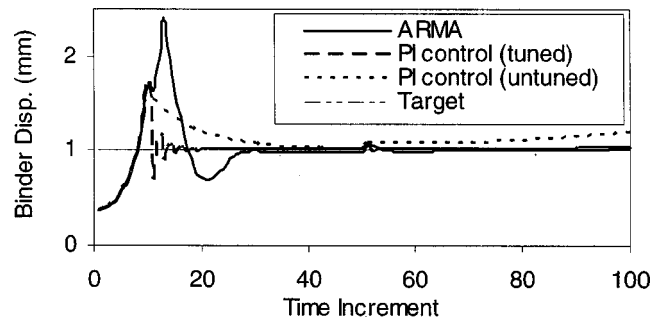


**Fig. 5 Binder displacements using ARMA model, tuned PI control and untuned PI control**

arbitrarily, to reflect the general trend displayed by the binder displacement when the binder force or the punch displacement is changed. The constants in the objective function were obtained through curve fitting. Also, to study the adaptive behavior of the two strategies, the objective function was defined differently in two separate domains i.e., from time increment 1 to 50 and from time increment 51 to 100. This represented a change in the parameters of the system, thus enabling us to observe the tracking ability of the two methods. The simulation was run for 100 increments and the objective function was defined as follows:

For increment numbers from 1 to 50,

$$BD = 2.42856 * e^{(-0.000194 * BF)} \quad (11)$$

For increment numbers from 51 to 100,

$$BD = 2.42856 * e^{(-0.000194 * BF)} + 0.6 * (T_n)^3 \quad (12)$$

where

$BD$  = binder displacement in mm,

$BF$  = binder force in  $N$ ,

$T_n$  = normalized punch displacement, (varies linearly from 0 to 1 over 100 increments)

For the purpose of this simulation, the target binder displacement was set at 1 mm. Figure 5 shows the result obtained using the ARMA model for prediction of binder force, and the same result obtained by using PI control. It was seen that the results from the ARMA model and the PI controller were comparable. Also, the PI control model tends to oscillate before settling on a converged value. This would lead to convergence difficulties in an FEM simulation. The corresponding binder force trajectories are shown in Fig. 6. The results shown for the PI control in Figs. 5 and 6 are "tuned" results. The values of proportional gain ( $K_p$ ) and integral gain ( $K_i$ ) had been adjusted for the best result, which was obtained at  $K_p = 820$  and  $K_i = 6040$ . The performance of the control system is sensitive to the values of  $K_p$  and  $K_i$ . Figures 5 and 6 also show the binder displacement and the binder force profile obtained for  $K_p = 500$  and  $K_i = 500$ . The results are clearly

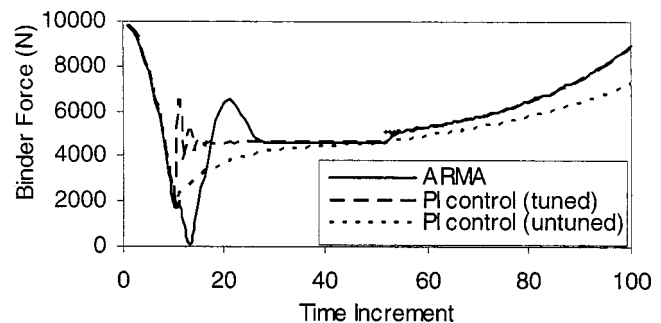


**Fig. 6 Calculated binder force profiles using ARMA, tuned PI control and untuned PI control**

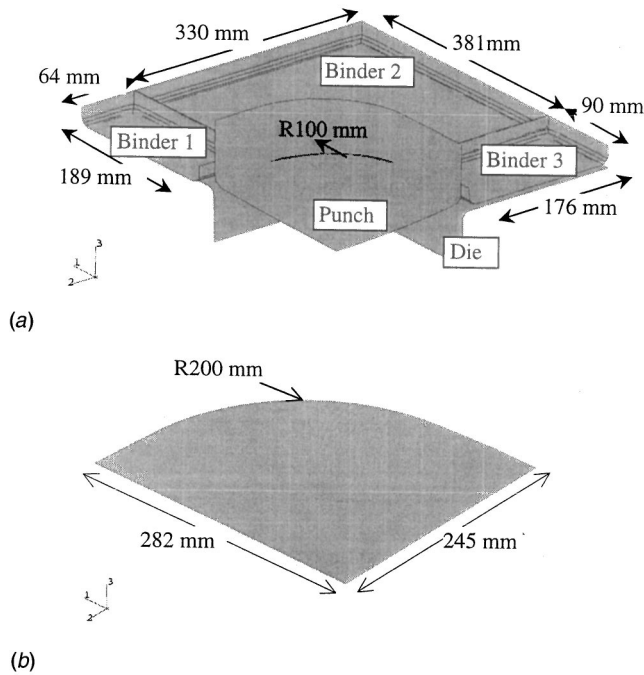


Fig. 7 (a) Schematic of one quarter of the tooling; (b) Schematic of one quarter of the blank

unsatisfactory. Physically  $K_p$  and  $K_i$  relate to the material stiffness, structural stiffness, material resistance to wrinkling, etc. A change of material (e.g. aluminum v/s steel) could easily change the stiffness by 3 times. In addition, due to other factors, a change of optimal  $K_p$  by 10 times is realistic and reasonable. In comparison, the ARMA model is a more robust approach and does not require any such adjustment.

## 5 FEM Simulation: Rectangular Pan Forming

The strategy proposed in this work is validated by implementing it into a finite element simulation. The commercial finite element code ABAQUS/Standard is used for the simulation. Although explicit codes like ABAQUS/Explicit or LS-Dyna are more common in simulations of sheet metal forming, we use an implicit code because it offers the capability of incorporating the particular user element that we need for feedback control.

The problem analyzed here is a rectangular pan forming simulation with a segmented binder. One quarter of the pan is modeled in the simulation and appropriate symmetric boundary conditions are applied where necessary. The blank is modeled by using 4-node reduced-integration shell elements (S4R). The binders, die and punch are considered to be rigid bodies. The coefficient of friction between all the contacting surfaces is taken to be 0.125. This value is selected based on tests performed by Jalkh et al. [25]. A soft-contact friction formulation is used in the finite element simulation to aid convergence. The blank is considered to be aluminum sheet of thickness 1.1 mm. The material is modeled as an elastic-plastic material with a von-Mises yield surface following the isotropic hardening law. The elastic properties of the material are the Young's modulus,  $E$ , of 70 GPa and Poisson's Ratio,  $\nu$ , of 0.33. The plastic behavior of the material is modeled using the Power law ( $\sigma = K\varepsilon^n$ ) with a strength coefficient,  $K$ , of 570 MPa and a strain hardening exponent,  $n$ , of 0.33. The material model used here is not the best for aluminum. However, the purpose of this paper is to demonstrate a strategy for obtaining a variable binder force history. The same strategy should work for a different material model. Figures 7(a) and 7(b) show schematics of the tooling and the blank, respectively. The corner radii for the die and the punch are 8 mm each and a gap of 1.9 mm is main-

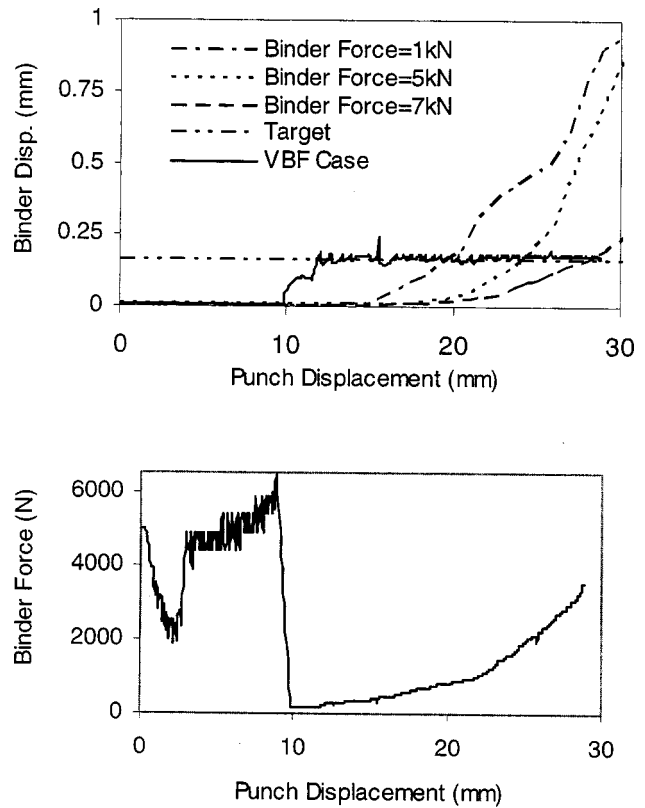


Fig. 8 Binder Displacements for constant binder forces and variable binder force applied on Binder 1 and the corresponding variable binder force profile. Forces on Binder 2 and Binder 3 are kept constant at 10 kN and 5 kN, respectively.

tained between the die and the punch. The segmented binder is composed of three parts, shown as Binder 1, Binder 2 and Binder 3 in Fig. 7.

The binder force on the binders will be variable, and they will be predicted by the ARMA model. The proposed strategy is implemented by creating a user-defined element which applies a binder force prescribed by the ARMA model, based on the value of binder displacement. The user-defined element has only one degree of freedom, i.e. binder displacement in the 3-direction. The reaction force on that degree of freedom is the binder force applied. Wrinkling occurs due to a relatively low binder force in the presence of a certain compressive stress level. On the other hand, a high restraining force applied on the binder would restrict the material flow and lead to tearing failure near the punch radius. Therefore, a control algorithm that allows the binder force to change such that it just suppresses the wrinkling tendency should give a better result than an optimal constant binder force. The initial value of binder force on each binder is set at a high value. The binder force rapidly decreases from this initial value and allows material to draw in without wrinkling. When the buckling amplitude at a particular binder reaches a predetermined critical value, the corresponding binder force increases to suppress the wrinkling tendency. When the amplitude is lower than the specified value, the binder force remains constant allowing more material to be drawn into the free section in order to delay potential tearing failure.

**5.1 Simulation Results: Case 1.** The first case of results presented here is for a simulation where the variable blank holder force algorithm is applied to a single binder. In Fig. 7(a), the blank holder forces on Binder 2 and Binder 3 are kept constant at 10 kN and 5 kN, respectively, and the blank holder force on Binder 1 is varied according to the ARMA model. Figure 8 shows the calcu-

**Table 1 Maximum Principal Strain at Punch Radius for various cases when binder forces on Binders 2 and 3 are kept constant at 10 kN and 5 kN, respectively**

Binder force Case	Constant 1 kN	Constant 5 kN	Constant 7 kN	Variable Binder Force
Maximum Principal strain at Punch Radius under Binder 1 Punch	8.1%	9.8%	10.1%	9.1%
Displacement at which wrinkling is initiated	15 mm	18 mm	19 mm	controlled

lated variable binder force (VBF) profile and the corresponding binder displacement. The binder displacement is restricted to a prescribed value of 0.16 mm, which corresponds to about 15% of the sheet thickness.

For comparison, three constant binder force cases are also presented in Fig. 8. In each of these cases, the force on Binder 1 is kept constant at 1 kN, 5 kN and 7 kN, respectively. The onset of wrinkling is clearly seen in the 1 kN and 5 kN cases. Table 1 lists the resulting maximum principal strain at the punch radius under Binder 1 in all these cases. It can be seen that the strain is lower in the variable binder force case than the 5 kN and 7 kN cases. If a lower value of constant binder force is applied, e.g. 1 kN, the strain obtained is lower than the VBF case, however, wrinkling is initiated much earlier, at a punch displacement of about 15 mm compared to 18 mm, 19 mm and the controlled level in the 5 kN, 7 kN and VBF cases. The best result among all the cases is one that achieves a reasonable trade-off between wrinkling and tearing. The VBF case allows the sheet to thicken or wrinkle, and yet, controls the wrinkling amplitude to an acceptable level. This allows more material to flow into the unsupported region; therefore, tearing failure is delayed. At this juncture, we would like to reiterate that the variable binder force does not eliminate or suppress wrinkling, but merely controls it to an acceptable level. In comparison to the 7 kN case, the maximum binder force in the VBF case is less than 7 kN. This would suggest that wrinkles should appear earlier in the VBF case, where the maximum binder force is around 6 kN, than the 7 kN case (19 mm). At first glance, this appears to be a contradiction. In hindsight, however, we realize that wrinkling for the VBF case is initiated at a punch stroke of approximately 10 mm, which is much earlier than the case of the 7 kN binder force. It is after this initiation of wrinkling that the wrinkling amplitude is maintained at a constant level of 0.16 mm, whereas, in the CBF case, it continues to rise.

**5.2 Simulation Results: Case 2.** The second case of results presented here is for a simulation in which the blank holder forces on Binder 1, Binder 2 and Binder 3 are controlled using the variable binder force algorithm. The model used in this case is the same as the one used in the previous case. The binder forces on all three binders are controlled using the ARMA model. Figure 9 shows the binder displacement for Binders 1, 2 and 3 respectively. The maximum allowable binder displacement is 0.16 mm, which corresponds to about 15% of the sheet thickness. Figure 10 shows the corresponding binder force profiles. At this point we would like to reiterate that the binder force profiles shown in the figures correspond to one quarter of the blank. The blank holder force for the entire blank is obtained by scaling up these values accordingly. The initiation of wrinkling can clearly be seen at a punch displacement of 4 mm for Binder 1 and Binder 2, and about 5 mm for Binder 3. The binder force profiles also reflect the wrinkling tendency of the blank. The region of the blank under Binders 1 and 2 shows a strong tendency to wrinkle and so the binder force reaches a maximum value of 8.72 kN for Binder 1 and 6.42 kN

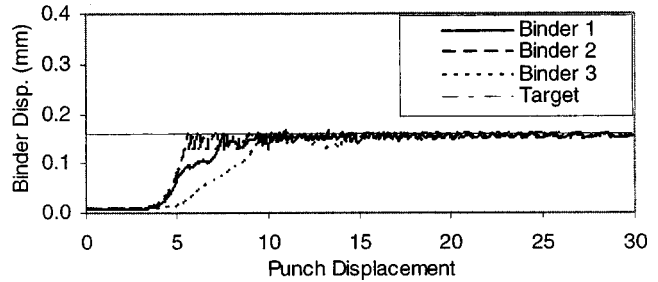


**Fig. 9 Binder displacements for binders 1, 2 and 3 subjected to a variable binder force obtained using an ARMA model**

for Binder 2. The corresponding values of blank holder pressure acting on the blank in these regions are 1.96 MPa and 0.42 MPa. The blank area under Binder 3 does not show a strong tendency to wrinkle and therefore, the binder force at Binder 3 reaches a maximum value of only 2.64 kN (0.39 MPa blank holder pressure). The wrinkling tendency is also reflected in the values of compressive stress that develop in the flange. The maximum compressive stress in the flange under Binder 1 is 275 MPa in the circumferential direction along the flange and 103.7 MPa (compressive) in the radial direction. The corresponding values for Binder 2 are 246 MPa and 176 MPa (both compressive). The region of the blank under Binder 3 has a maximum circumferential compressive stress of 205 MPa and a radial compressive stress of 2.7 MPa. The portion of the flange under Binder 3 shows the least tendency to wrinkle, and correspondingly, the compressive stresses in this area are the lowest. The regions of the flange under Binder 1 and Binder 2 show a more pronounced wrinkling tendency which is reflected by the high compressive stresses developed in these areas.

## 6 FEM Simulation: Hemispherical Punch With Tailor Welded Blank

Cases 1 and 2 utilized the same ARMA model (Eq. (8)) to obtain the optimal blank holder force profiles for one binder and three binder cases for rectangular cup forming. In this section, we shall demonstrate the applicability of the same model to a different forming problem, i.e., the forming of a tailor-welded blank using a hemispherical punch. The blank consists of two sheets of AKDQ steel welded together. The thicker sheet has a thickness of 1.52 mm and the thinner sheet is 0.84 mm thick. Both sheets have the same elastic material properties, i.e. Young's modulus,  $E$ , of 206 GPa and Poisson's Ratio,  $\nu$ , of 0.3. The plastic behavior of the material is, once again, modeled using the Power law ( $\sigma = K\varepsilon^n$ ). The thicker material has a strength coefficient,  $K$ , of 542 MPa and a strain hardening exponent,  $n$ , of 0.22, while the corresponding values for the thinner material are 563 MPa and 0.23, respectively. One half of the geometry is modeled to take advan-

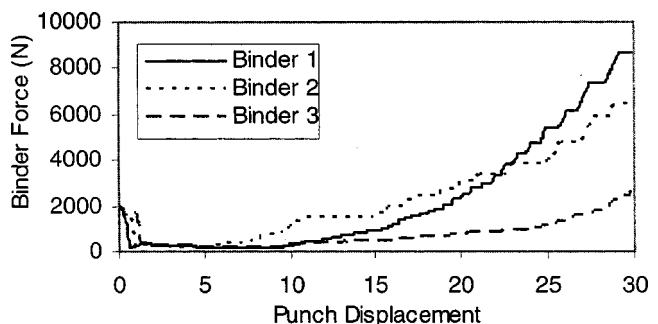


**Fig. 10 Variable blank holder force profiles for Binders 1, 2 and 3**

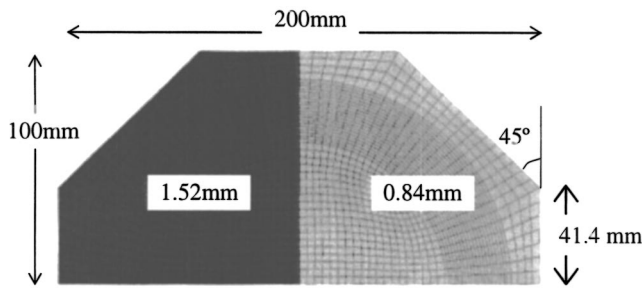


Fig. 11 Schematic of one half of the blank used in tailor welded blank forming (Case 3)

tage of the symmetric nature of the problem. Figure 11 shows a schematic of the blank. The punch is a hemisphere of radius 50 mm. The die cavity and the binder have radii of 54 mm, thus ensuring a gap of 4 mm between them and the closest portion of the punch at its lowest point. A schematic of the tooling is shown in Fig. 12. As seen in the figure, the binder is segmented into two parts called Binder 1 and Binder 2. Binder 1 applies a blank holder force to the thick sheet and Binder 2 does the same to the thin sheet. The binder and die fillet radii are 5 mm each. All other features of the simulation are the same as in the case of the rectangular pan forming discussed in the previous section. The ARMA model of the same structure as before is used to control the blank holder forces on Binder 1 and Binder 2, respectively.

**6.1 Simulation Results: Case 3.** Figure 13 shows the binder displacement plots for the Binders 1 and 2. The flange wrinkling for Binder 1 and Binder 2 are successfully controlled to values of 0.23 mm and 0.13 mm, respectively. These values correspond to approximately 15% of the sheet thickness. The corresponding BHF profiles are shown in Fig. 14. The values depicted here are obtained for one half of the blank. The binder force on the thicker portion of the blank (Binder 1) increases gradually to a

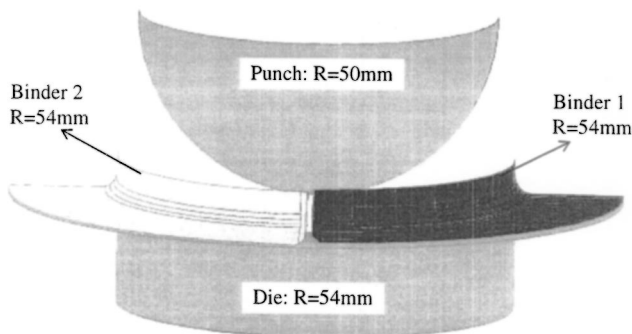


Fig. 12 Schematic of one half of the tooling used in case 3

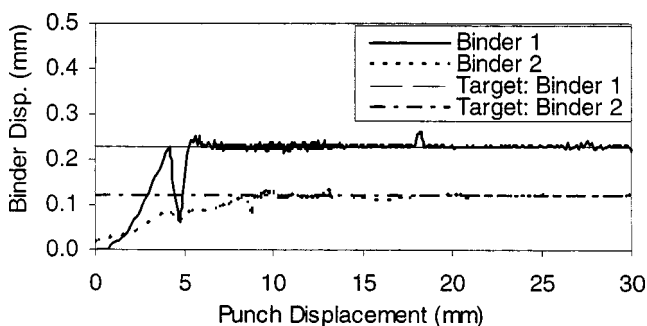


Fig. 13 Binder displacements for Binder 1 and Binder 2 in case 3

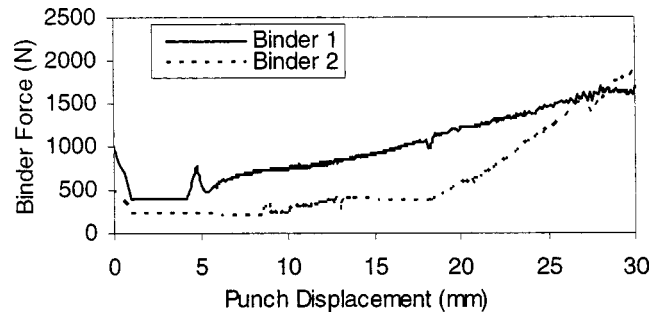


Fig. 14 Binder force profiles for Binder 1 and Binder 2 in case 3

value of about 1.7 kN. The force on the thinner portion of the blank (Binder 2) however, shows quite a different trend. This binder force increases gradually at first, then decreases slightly and increases quite sharply in the end to reach a value of about 2 kN. In Fig. 13, a spike can be seen in the binder displacement plot for Binder 1. This can be attributed to the tendency of the ARMA model to overshoot the target before settling down to a converged result (as seen in Fig. 5). The spike can be ignored in a practical scenario.

## 7 Discussions and Conclusion

In this paper, we have proposed a strategy where the ARMA model is used to estimate the optimum blank holder force trajectory in order to control wrinkling to a predetermined acceptable level. This strategy ensures that the binder force applied on the blank is just sufficient to suppress the wrinkling tendency and therefore, allows more material to be drawn into the forming area which in turn, reduces the chances of tearing failure. The key technical contribution of this work lies in the fact that the strategy can be applied to multiple blank holder force scenarios. Also, due to the generic nature of the ARMA model, the controller does not require any tuning as seen when conventional methods like PI controllers are used. The model does not require any *a-priori* information about the system and it can be used with different kinds of tooling conditions, part geometries and material models. The strategy has been verified by implementing it into an FEM simulation where a rectangular part is formed using segmented binders, and in the forming of a tailor welded blank using a hemispherical punch. As is evident in the results the ARMA model can be successfully used to predict the blank holder force trajectory. At this juncture, we would like to emphasize the fact that this strategy does not eliminate wrinkling, but merely restricts it to an acceptable value.

The initial portion of the binder force plot in Fig. 8, up to a punch displacement of 10 mm, shows that the binder force changes even though the wrinkling amplitude is low. The blank does not show a tendency to wrinkle during this period. However, the control algorithm keeps varying the binder force in an attempt to achieve the target binder displacement. This tendency is suppressed in subsequent simulations, where the algorithm is modified such that the binder force variation does not start unless the blank starts to wrinkle. In order to improve convergence, the code for the user element has been structured in such a manner that control happens only when the actual binder displacement is beyond a small acceptable range around the target value. This gives rise to the stepped binder force trajectory in Fig. 10. However, this should not cause any problems in the actual implementation of the strategy. The binder force trajectory estimated from simulations in this closed loop manner can then be smoothed and used in an actual forming simulation.

We also investigated the effect of coupling the various inputs and outputs to create a model which captures dependence between binder displacement and binder force on different binders. In other

words, we tried to account for the fact that the variation of blank holder force on Binder 1 might affect the wrinkling amplitude of the blank under Binder 2. This approach does not give any significant improvement in results, and dramatically increases the number of parameters that need to be identified (39 v/s 15).

Our prime concern in this research endeavor was the suppression of flange wrinkling. Other failure modes such as sidewall wrinkling and tearing were not considered. These particular failure modes need to be addressed in situations where they appear as the dominant means of failure. This was observed in the case of the hemispherical punch. Although the flange wrinkling had been restricted to an acceptable value, the deformed blank clearly showed the appearance of sidewall wrinkling in the thinner portion of the blank. This is due to the fact that a large region of the blank is unsupported in the initial stages of punch displacement and the binder forces required to suppress sidewall wrinkling are far higher than those required to suppress flange wrinkling. The generic nature of the model also means that it can be employed to suppress sidewall wrinkling. The only change that needs to be made in the algorithm is that the binder displacement (used as a measure of flange wrinkling) which is treated as the system input needs to be replaced with a suitable parameter that effectively measures the sidewall wrinkling tendency. The methodology discussed herein can be applied to tearing failure as well. This is currently under investigation.

The results obtained from the finite element simulation indicate that the ARMA model can be effectively used in multiple binder force scenarios. This strategy can easily be coupled with other emerging technologies like tailor welded blanks in order to obtain improved part quality.

## Acknowledgments

The support from NSF grant (DMI-9703249) is greatly appreciated.

## Nomenclature

$BD_i$	= binder displacement in the $i$ th increment
$BF_i$	= Binder force in the $i$ th increment
$DBF_i$	= Binder force change in the $i$ th increment
$E$	= Young's Modulus
$K$	= Strength coefficient
$K_i$	= Integral gain
$K_p$	= Proportional gain
$\mathbf{P}_n$	= System information matrix in the $i$ th increment
$T_i$	= Normalized punch displacement in the $i$ th increment
$\mathbf{a}_p$	= Parameters for the autoregressive part of the ARMA model
$\mathbf{b}_q$	= Parameters for the moving average part of the ARMA model
$d$	= Time delay between input and output
$e_i$	= Error between actual binder displacement and target in the $i$ th increment
$err$	= Estimation error
$i$	= Increment number/sampling interval
$n$	= Strain hardening exponent
$s$	= Number of autoregressive terms in ARMA model
$t$	= Number of moving average terms in ARMA model
$\mathbf{x}_i$	= System input in the $i$ th increment
$\mathbf{y}_i$	= System output in the $i$ th increment
$y$	= Actual system output
$\hat{y}$	= Predicted system output
$\alpha$	= Initializing constant
$\lambda$	= Forgetting factor
$\nu$	= Poisson's Ratio

$\theta_j$	= Parameters of the system ( $j=1$ to 5)
$\boldsymbol{\theta}_i$	= vector of system parameters in the $i$ th increment
$\boldsymbol{\psi}_i$	= vector of system inputs in the $i$ th increment

## References

- [1] Ahmetoglu, M. A., Coremans, A., Kinzel, G. L., and Altan, T., 1993, "Improving Drawability by Using Variable Blank Holder Force and Pressure in Deep Drawing of Round and Non-Symmetric Parts," SAE Technical Paper No. 930287, Warrendale, PA.
- [2] Kergen, R., and Jodogne, P., 1992, "Computerized Control of Blank Holder Pressure on Deep Drawing Presses," SAE Technical Paper No. 920433, Warrendale, PA.
- [3] Cao, J., and Boyce, M. C., 1997, "A Predictive Tool for Delaying Wrinkling and Tearing Failures in Sheet Metal Forming," ASME J. Eng. Mater. Technol., **119**, pp. 354–365.
- [4] Cao, J., Kinsey, B., and Solla, S. A., 2000, "Consistent and Minimal Springback Using a Stepped Binder Force Trajectory and Neural Network Control," ASME J. Eng. Mater. Technol., **122**, pp. 113–118.
- [5] Liu, G., Lin, Z., Bao, Y., and Cao, J., 2002, "Eliminating Springback Error in U-Shaped Part Forming by Variable Blank Holder Force," J. Mater. Eng. Perform., **11**(1), pp. 64–70.
- [6] Siegert, K., Wagner, S., and Zeigler, M., 1996, "Closed Loop Binder Force Systems," SAE Technical Paper No. 960824.
- [7] Neugebauer, R., Leib, U., and Braunlich, H., 1997, "Influence of Material Flow in Deep Drawing Using Individual Controllable Draw Pins and Smooth Blank Holder Design," SAE Technical Paper No. 970989.
- [8] Doege, E., Eland, L.-E., and Ropers, C., 1999, "Pliable Blank Holder Systems for the Optimization of Process Conditions in Deep Drawing," Adv. Technol. Of Plasticity, *Proceedings of the 6th ICTP*, Sept. 19–24, pp. 177–182.
- [9] Kinsey, B., Liu, Z., and Cao, J., 2000, "A Novel Forming Technology for Tailor-Welded Blanks," J. Mater. Process. Technol., **99**, pp. 145–153.
- [10] Shulkin, L., Jansen, S. W., Ahmetoglu, M. A., Kinzel, G. L., and Altan, T., 1996, "Elastic Deflections of the Blank Holder in the Deep Drawing of Sheet Metal," J. Mater. Process. Technol., **59**(1–2), pp. 34–40.
- [11] Hardt, D. E., and Lee, C. G. Y., 1986, "Real-Time Control of Sheet Stability During Stamping," *Proceedings of the 13th North American Manufacturing Research Conference*, Society of Manufacturing Engineers, Dearborn, MI, pp. 315–322.
- [12] Kergen, R., and Jodogne, P., 1992, "Computerized Control of Blank Holder Pressure on Deep Drawing Presses," Society of Automotive Engineers Technical Paper No. 920433, Warrendale, PA.
- [13] Kergen, R., 1993, "Closed Loop Control of Blank Holder Force Based on Deep Drawing Parameters: Its Laboratory and Industrial Applications," ID-DRG Working Group, Linz, Austria.
- [14] Hirose, Y., Kojima, M., Ujihara, S., and Hishida, U., 1992, "Development of Forming Techniques With Real-Time Control of Blank Holding Force," *Proceedings of the 17th Biennial Congress of the IDDRG*, pp. 300–307.
- [15] Kirii, K., Shinabe, M., Hirabayashi, Y., and Akiyama, M., 1995, "Binding Force Control of Uni-Pressure Cushion in Automobile Panel Stamping," Society of Automotive Engineers Technical Paper No. 950916, Warrendale, PA.
- [16] Ahmetoglu, M. A., Coremans, A., Kinzel, G. L., and Altan, T., 1993, "Improving Drawability by Using Variable Blank Holder Force and Pressure in Deep Drawing of Round and Non-Symmetric Parts," Society of Automotive Engineers Technical Paper No. 930287, Warrendale, PA.
- [17] Ahmetoglu, M. A., Broek, T., Kinzel, G. L., Altan, T., and Chandrokar, K., "Deep Drawing of Rectangular Pans From Aluminum Alloy 2008-T4," Society of Automotive Engineers Technical Paper No. 950694, Warrendale, PA.
- [18] Sim, H. B., and Boyce, M. C., 1992, "FEM Analysis of Real-Time Stability Control in Sheet Forming Processes," ASME J. Eng. Mater. Technol., **114**, pp. 180–188.
- [19] Siegert, K., and Ziegler, M., 1997, "Pulsating Blank Holder Force," Society of Automotive Engineers Technical Paper No. 970987, Warrendale, PA.
- [20] Hsu, C.-W., Ulsoy, A. G., and Demeri, M. Y., 2000, "An Approach for Modeling Sheet Metal Forming for Process Controller Design," ASME J. Manuf. Sci. Eng., **122**, pp. 717–724.
- [21] Graupe, D., Krause, D. J., and Moore, J. B., 1975, "Identification of Autoregressive Moving-Average (ARMA) Parameters of a Time Series," IEEE Trans. Autom. Control, **AC-20**(1), pp. 104–107.
- [22] Kay, S. M., and Marple, S. L., Jr., 1981, "Spectrum Analysis—A Modern Perspective," *Proceedings of IEEE*, **69**(11), pp. 1380–1414.
- [23] Fassois, S. D., Eman, K. F., and Wu, S. M., 1989, "A Fast Algorithm for On-Line Machining Process Modeling and Adaptive Control," ASME J. Eng. Ind., **111**, pp. 133–139.
- [24] Graupe, D., 1984, *Time Series Analysis, Identification and Adaptive Filtering*, Robert E. Krieger Publishing Company, Malabar, Chap. 5, pp. 70–88.
- [25] Jalkh, P., Cao, J., Hardt, D., and Boyce, M. C., 1993, "Optimal Forming of Al 2008-T4 Conical Cups Using Force Trajectory Control," Journal of Materials & Manufacturing, **102**, Sec. 5, pp. 416–427.